Semiconductor Physics, Quantum Electronics & Optoelectronics. 1999. V. 2, N 4. P. 31-36.

PACS: 71.28, 72.20.J, 78.40.F, 78.66

Characterization of $Hg_{1-x}Mn_xTe$ single crystals and $Hg_{1-x}Mn_xTe$-based photodiodes

L.A. Kosyachenko, I.M. Rarenko, O.O. Bodnaruk, V.M. Frasunyak, V.M. Sklyarchuk, Ye.F. Sklyarchuk, Sun Weiguo*, Lu Zheng Xiong*

Chernivtsi University, Kotsyubinsky Str. 2, 274012 Chernovtsi, Ukraine

** Luoyang Optoelectronics Institute, PO Box 030, 471009 Luoyang, Henan, P.R. China, E-mail (L.A.K.): oe-dpt@phys.chsu.cv.ua*

Abstract. The results of electrical, Hall effect and optical absorption studies of $Hg_{1-x}Mn_xTe$ ($x >> 0.1$–0.2) single crystals in the temperature range 80 to 300 K are reported. The observed dependences of the Hall coefficient inversion temperature on the acceptor concentration and semiconductor bandgap are supported by calculations. The long-wavelength absorption edge is treated using the Kane model. The revealed features of the absorption are considered to be caused by small effective mass of electrons in the narrow-gap semiconductors studied. The diodes with *p-n* junctions produced by ion etching have good rectifying properties determined by carrier generation-recombination, tunneling and avalanche processes.

Keywords: narrow-gap semiconductors, electrical and optical properties, photodiodes.

Paper received 05.10.99; revised manuscript received 13.12.99; accepted for publication 17.12.99.

1. Introduction

$Hg_{1-x}Mn_xTe$ alloy is known to be a promising material for infrared detectors. There are reasons to believe that stability and reproducibility of the $Hg_{1-x}Mn_xTe$ photodiodes can be improved as compared to those of the well-studied $Hg_{1-x}Cd_xTe$ devices [1-3]. Early in the previous works the electrical and optical properties of $Hg_{1-x}Mn_xTe$ in zero magnetic field were demonstrated to be analogous in many respects to $Hg_{1-x}Cd_xTe$ [4, 5]. The characteristics of infrared-sensitive *p-n* junction on these materials are also similar [3, 6]. However, by now the primary emphasis in the paper devoted to $Hg_{1-x}Mn_xTe$ is focused on magnetooptical effects, quantum structures, phenomena observed at very low temperatures, etc. Experimental data required to provide an explanation for the photodiode performance are scarce and predominantly qualitative. The purpose of this paper is this deficiency in such information to compensate to some extent. We report the $Hg_{1-x}Mn_xTe$ diode characteristics along with electrical and optical properties of the material ($x = 0.1$–0.2) in the important range of temperatures (80–300 K).

2. Electrical and Hall measurements

Single-crystalline $Hg_{1-x}Mn_xTe$ was grown by a modified Bridgman technique followed by annealing in Hg vapor [7]. To produce *p-n* junction, the ion etching of *p*- $Hg_{1-x}Mn_xTe$ was used. Fabrication of the multielement photodiode arrays involved photolithography, surface passivation, antireflection coating and three-layer Au/Cr/Pd/$Hg_{1-x}Mn_xTe$ metallization processes [8, 9].

As-grown $Hg_{1-x}Mn_xTe$ ($x = 0.1$–0.2) alloys have generally *p*-type conductivity at low temperatures (80 K), and the conductivity of the alloys, σ, ranges conventionally within 10 to 100 $Ohm^{-1}cm^{-1}$. As temperature elevates to 300 K, *p*-to-*n* conversion usually occurs, and σ can increase more than order of magnitude, or first somewhat decreases and then increases, smootly or drastically. For relatively low-resistance material *p*-to-*n* conversion occurs at temperatures up to 300 K or above while for more high-resistance material (as-grown or annealed in Hg vapor for a long time) the conversion temperature turns out below 80 K. As an illustration, Fig. 1 shows the temperature depen-dences of Hall coefficient R_H for the samples different widely in this respect. The measurements of R_H were carried out under 0.136 T magnetic field strength where the electrical properties of the samples leave to be unchanged.

A plausible explanation for the observed $R_H(T)$ and $s(T)$ curves can be obtained on the basis of simplified model taking into account a dramatic difference between electron and hole mobilities, μ_n and μ_p, in narrow-gap $Hg_{1-x}Mn_xTe$. Denote the acceptor (Hg vacancies) concentration and unknown donor concentration by N_a and N_d, and the energy depth of the corresponding levels by E_a and E_d, respectively. Denoting the energy distance between the Fermi level and the top of the valence band by $\Delta\mu$, we will write the condition of electrical neutrality as

© 1999, Institute of Semiconductor Physics, National Academy of Sciences of Ukraine

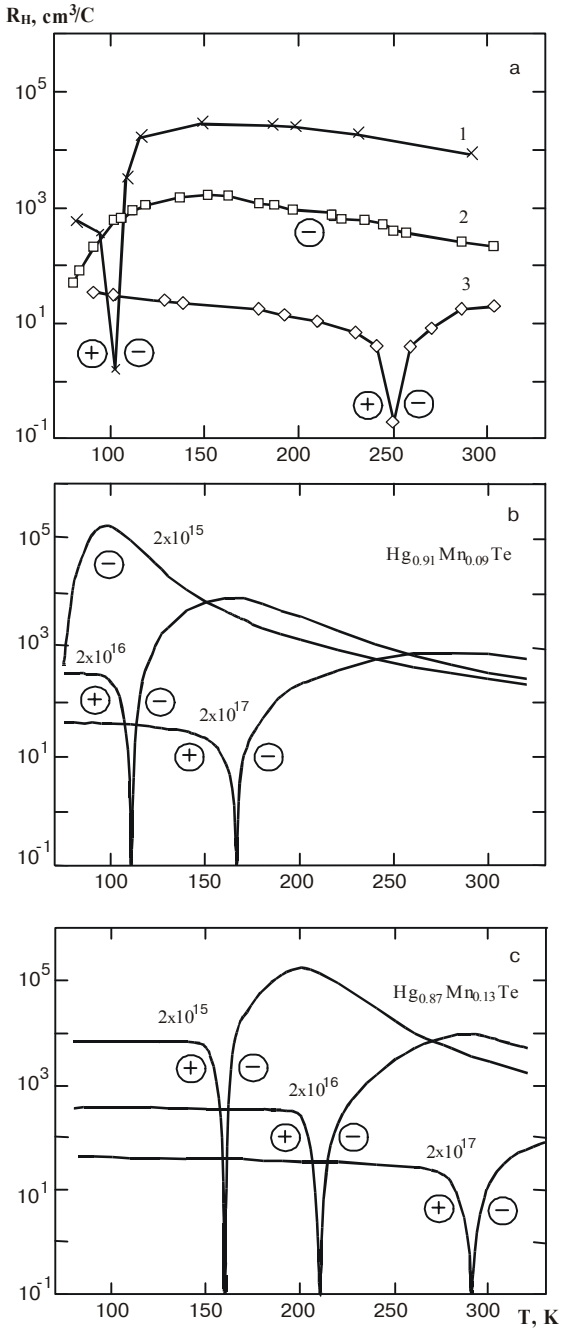

Fig. 1. Representative temperature dependencies of the Hall coefficient for different acceptor concentrations (in cm^{-3}): measured for two $Hg_{1-x}Mn_xTe$ crystals (a), calculated for $Hg_{0.91}Mn_{0.09}Te$ (b) and $Hg_{0.87}Mn_{0.13}Te$ (c).
The donor concentration is 10^{15} cm^{-3}, $\mu_p = \mu_n / 100$.

$$N_c \frac{2}{\sqrt{2\pi}} \int_0^{Z\max} \frac{\sqrt{z}}{\exp\left(z + \frac{E_g - \Delta\mu}{kT}\right)+1} dz + \frac{N_a}{2\exp\left(\frac{E_a - \Delta\mu}{kT}\right)+1} = \frac{N_v}{\exp\left(\frac{\Delta\mu}{kT}\right)+1} + \frac{N_d}{2\exp\left(\frac{E_d + \Delta\mu - E_g}{kT}\right)+1}, \quad (1)$$

where the Fermi integral makes allowance for a possibility of degeneracy of the electron gas in the conduction band (for sufficient accuracy the upper limit of integration over $z = E/kT$ can be set as large as 20–30); N_c and N_v are the effective density of states in the conduction and valence bands which can be considered as the parabolic ones, i.e. $N_c = 2(m_e kT/2\pi\hbar^2)^{3/2}$ and $N_v = 2(m_h kT/2\pi\hbar^2)^{3/2}$. The factors 2 at exponents take into account the degeneracy of the impurity energy levels. For the effective masses of electrons, m_e, and holes, m_h, as well as for the energy bandgap, E_g, we will use the "standard" relationships [3]:
$m_e = 5.7\cdot10^{-16} E_g m_o/P^2$, $\quad m_h = 0.5 m_o$,
$E_g = -0.253 + 3.44x + 4.9\cdot10^{-4}T - 2.55\cdot10^{-3}xT$,
where P is the energy band parameter of the Kane theory [10] equal to $(6.461 - 0.121x)\cdot10^{-8}$ [eV cm] for $Hg_{1-x}Mn_xTe$ [3]. Taking E_a and E_d equal to 0.005 eV [11], one can obtain $\Delta\mu$ for given N_a, N_d and T, and then, knowing $\Delta\mu$, compute the electron and hole concentrations in the bands, n and p, and finally compute the Hall coefficient for the case of the mixed nature of conduction

$$R_H = \frac{1}{e}\frac{p\mu_p^2 - n\mu_n^2}{(n\mu_n + p\mu_p)^2} = \frac{1}{e}\frac{p - nb^2}{(p + nb)^2}, \quad (2)$$

where $b = \mu_n/\mu_p$ is the ratio of the electron and hole mobilities equal to 10^2 for $Hg_{1-x}Mn_xTe$ [3].

The temperature dependences of the Hall coefficient calculated using Eq. (2) for $Hg_{0.91}Mn_{0.09}Te$ and $Hg_{0.87}Mn_{0.13}Te$, i.e. alloys suitable for infrared detection in the 3-5 and 8–14 μm atmospheric windows are shown in Fig. 1(b) and 1(c). The curves are obtained for the N_a values varying in a wide range while the N_d value was taken to be 10^{15} cm^{-3} for all cases. Knowing of $\Delta\mu$ in the whole temperature region it is also possible to calculate the T dependences of the conductivity as $\delta = e(n\mu_n + p\mu_p)$ with the expression for μ_n in the form [3]

$$\mu_n = 9\times10^8 \left(\frac{0.095}{x}\right)^{7.5} T^{-2\left(\frac{0.095}{x}\right)^{0.6}}, \quad (3)$$

and taking as mentioned above $\mu_p = \mu_n/100$.

As can be seen from Fig. 1 and 2, the curves calculated for different acceptor concentrations N_a cover the whole variety of the observed $R_H(T)$ and $\sigma(T)$ dependences. It is worth noting that at all N_a the electron concentration is much less than the hole concentration (exclusive of the intrinsic conduction region at or above ~300 K). The p-to-n inversion of the Hall coefficient, occurring more easily for small N_a and E_g, is explained naturally by the vastly greater mobility of electrons as compared to that of holes while the non-monotonic i.e. dependence $\sigma(T)$ - by increasing the contribution of electrons to charge transport with concurrent decreasing the carrier mobilities when temperature elevates.

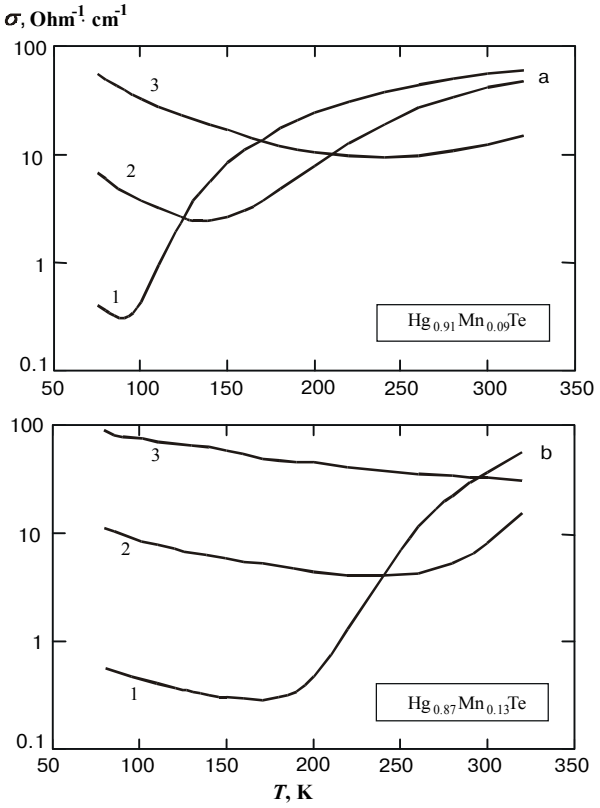

Fig. 2. Temperature dependences of conductivity for $Hg_{0.91}Mn_{0.09}Te$ and $Hg_{0.87}Mn_{0.13}Te$ calculated for different acceptor concentrations in cm^{-3}: *1* — $2\cdot10^{15}$, *2* — $2\cdot10^{16}$ and *3* — $2\cdot10^{17}$.

3. Optical absorption in $Hg_{1-x}Mn_xTe$ crystals

The optical constants of the crystals were found from the transmission curves of the planar surface-mirrored wafers. To obtain the absorption curves in a wide spectral range, a set of wafers with different thickness from 0.8–1.5 mm to 50–60 μm were used. This provided a reasonably accurate determination of the absorption coefficient α in the range from a few cm^{-1} up to several thousands of cm^{-1}. Experimental results obtained using infrared spectrometer (Model 29) were processed with allowance made for multiple reflections in a sample.

Fig. 3 shows some characteristic examples of the optical absorption curves for $Hg_{1-x}Mn_xTe$. One can see that all the curves exhibit relatively weak photon energy dependence in the low-energy region which transforms to sharply increasing portion of the curve as the photon energy stands out above a certain value. There is reason to believe that the former is associated with a free-carrier absorption while the latter is due to intraband transitions of electrons.

Theoretical treatment of the optical absorption in the region of interband transitions for semiconductors like $Hg_{1-x}Mn_xTe$ is conventionally based on the well proved Kane model [10]. In the case of a narrow-gap semiconductor, it is rightly believed that the spin-orbit splitting Δ is large enough ($\Delta >> E_g$), and the hole effective mass is much larger than the effective electron mass ($m_h >> m_e$) [5]. In this approximation, the expression for the dispersion law in the valence band has the form $E_v(k) = \hbar^2k^2/2m_h$ while in the conduction band

$$E_c(k) = \frac{\hbar^2 k^2}{2m_e} + \frac{1}{2}\left[\eta(k) - E_g\right], \tag{4}$$

where $\eta(k) = (E_g^2 + 8/3P^2k^2)^{1/2}$ and k is a solution of the equation

$$h\nu = E_c(k) + E_v(k) + E_g . \tag{5}$$

Using the above expressions, the absorption coefficient for the transitions between the heavy-hole band and conduction band can be written as [12]

$$\alpha(h\nu) = \frac{C}{n} A\gamma^2 \frac{m_v}{m_o}\left(\frac{m_o}{m_e}\right)^{1/2} \times \left(\frac{E_g}{h\nu}\right)^{1/2} (h\nu - E_g)^{1/2} \quad [cm^{-1}], \tag{6}$$

where $C = 3.8\cdot10^5$ with energies measured in eV, n is the refractive index, $m_v = m_h m_o/(m_h + m_o)$, $\gamma = (1/2)(1+E_g/\eta)$ and $A = (2h\nu - E_g)/(2h\nu + m_v E_g/m_o)$. It is easy to verify that as $h\nu$ is close to E_g, the Eq. (6) reduces to the well-known expression

$$\alpha(h\nu) = \alpha_o\sqrt{h\nu - E_g}\,, \tag{7}$$

where α_o is the $h\nu$ independent value. Our calculations have shown that for α as large as ~10^3 cm^{-1}, the deviation from the parabolic law $E_c(k)$ can be neglected even for E_g as small as 0.05–0.1 eV (i.e. Eq. (7) can be used for $\alpha < 10^3$ cm^{-1}). With this in mind, the $\alpha(h\nu)$ dependences in Fig. 4 are replotted on the α^2 versus $h\nu$ coordinates to obtaine the straight lines. It can be seen that all the measured dependences do yield the straight lines in the 200–300 $cm^{-1} < \alpha <$ 700–800 cm^{-1} region with the cutoff on the $h\nu$-axis equal to E_g with a high degree of accuracy.

With a knowledge of the E_g value, it is next possible to

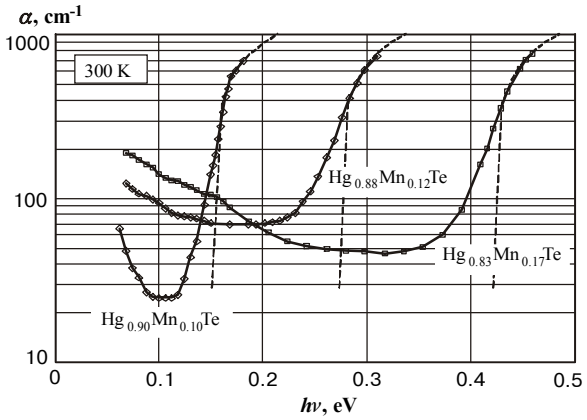

Fig. 3. Room-temperature absorption curves for $Hg_{1-x}Mn_xTe$ crystals with different Mn content.
The dashed lines show the curves calculated using Eq. (6)

calculate the $\alpha(h\nu)$ curves in a wide spectral range using the general formula (6). The dependences thus obtained are shown in Fig. 3 by dashed lines. (The calculated dependences are matched with the experimental points by adjusting the C value in Eq. (6)). One can see that good agreement between theory and experiment is observed in the region of the large value α up to 700–900 cm^{-1}. In the $\alpha < 100$–200 cm^{-1} region, the measured values of the absorption coefficient are seen to be in excess of the calculated ones. This can be accounted for by the presence of compositional fluctuation as well as inclusions with chemical content different from the base crystal. These are known to lead to the sloping blurred edge of the intrinsic absorption observed in a number of semiconductors.

The above model provides also an explanation for the variation of the $Hg_{1-x}Mn_xTe$ absorption curves with temperature. The key to understanding these changes seems to be lie in the temperature dependence of the semiconductor bandgap and, thereby in varying the electron effective mass. If the bandgap of the p-type $Hg_{1-x}Mn_xTe$ is wide enough, the temperature changes of the absorption curve are really reduced to the simple shift of the intrinsic absorption edge in the manner shown in Fig. 5. One can satisfy that as temperature elevates the bandgap widens in accordance to the relationship [3]

$$dE/dT = 4.9\cdot10^{-4} - 2.55\cdot10^{-3}\,x\,. \qquad (8)$$

An essentially another type of situation occurs in n-type $Hg_{1-x}Mn_xTe$ crystals, especially in the narrow-gap case. This is illustrated by a concrete example of the absorption curves presented in Fig. 6. As can be seen the absorption edge is shifted towards the smaller photon energy with the coefficient equal to $3.5\cdot10^{-4}$ eV K^{-1} when temperature decreases in the region of room temperature. According to Eq. (8) it corresponds to $x \approx 0.06$, i.e. to $E_g \approx 0.06$ eV at 300 K [3]. The observed room-temperature «bandgap» is in reality equal to 0.15–0.16 eV (see Fig. 6), i.e. far in excess of that followed from Eq. (8). To get out of difficulty, it should be assumed that the semiconductor with such a behavior is the degenerate one. In a case of degeneracy, the observed absorption edge is formed by the transitions of electrons from

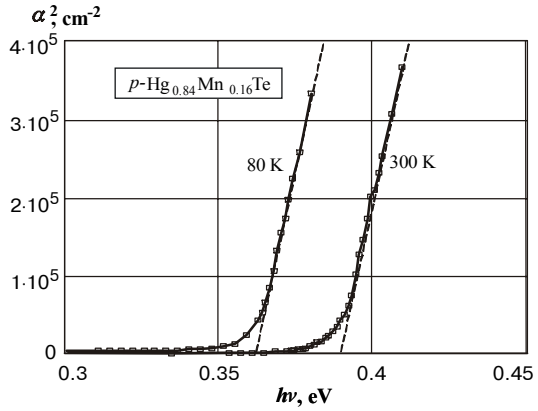

Fig. 5. Absorption curves for p-$Hg_{1-x}Mn_xTe$ crystal at different temperatures.
The dashed lines are the dependeces given by Eq. (7).

the valence band to the Fermi level instead of the bottom of conduction band (the Burstein-Moss effect). Taking the electron effective mass to be much smaller than the hole effective mass, i.e. $m_e m_h/(m_e+m_h) \approx m_e$, we can conclude that the Fermi level embedded into the conduction band by the energy equal to the difference between 0.15–0.16 eV and 0.06 eV, i.e., by ~ 0.1 eV at 300 K. This implies a *strong* degeneracy of a semiconductor, i.e. the case where the electron concentration depends only weakly on the temperature. Nevertheless, as the temperature decreases the electron effective mass also decreases due to the narrowing the bandgap. As a result, the absorption cross section of an electron increases giving arise the absorption coefficient to be also increased. These accounts for a drastic increase in optical absorption with decreasing T observed in the below-band-gap region (see Fig. 6).

4. $Hg_{1-x}Mn_xTe$ ion-etching photodiodes

The prospects of $Hg_{1-x}Mn_xTe$ alloy are known to be supported by experimental results achieved on *diffusion* and

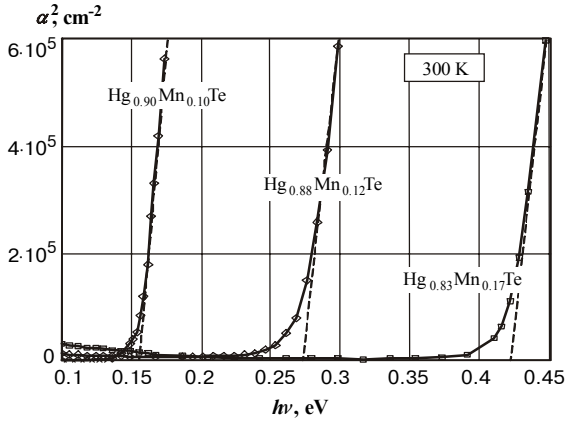

Fig. 4. Absorption curves are the same as in Fig. 1 but replotted on the α^2 *versus* $h\nu$ coordinates.

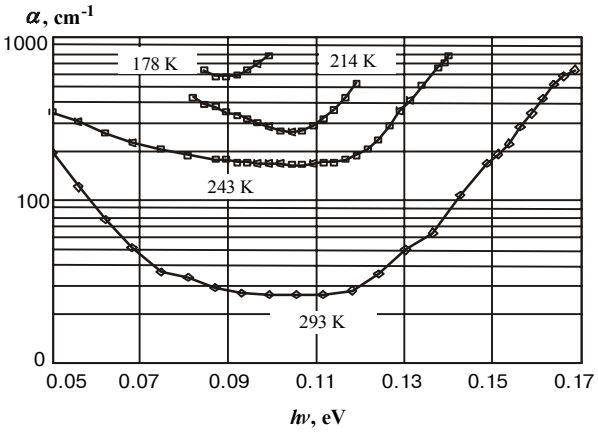

Fig. 6. The temperature variation of the absorption curve for degenerated n-$Hg_{1-x}Mn_xTe$ crystal.

ion-implanted p-n junction [4, 6, 14]. In this paper we present photodiodes with *p-n* junctions formed by *ion etching* (ion beam milling) of *p*- $Hg_{1-x}Mn_xTe$ [14]. This technique, used in current available microelectronics technology, is attractive because the ion etching is performed at relatively low ion energy (<1000 eV) and hence no damages in a crystal lattice is created (no post-etching annealing is required).

The Ar^+ ion beam milling was carried out in a common etch system for 1–1.5 min. As a result, the conduction of a layer near the crystal surface was transformed from *p*- to *n*-type with an electron concentration as high as ~10^{18} cm^{-3} while the hole concentration in the substrate was (2–5)·10^{16} cm^{-3}. The n^+-*p* junctions thus fabricated with Au/Cr/Pd ohmic contacts exhibit good rectifying properties and stability in time.

Fig. 7 shows the *I-V* characteristic of one of the $Hg_{0.91}Mn_{0.09}Te$ diodes at two temperatures. The distinguishing feature of the diode is that *at low forward biases* the *I-V* characteristic plotted on the ln*I* versus *V* coordinates yield the straight line with a slope equal to *e*/2*kT* indicating the recombination nature of the current. It can be seen from Fig. 7 that the temperature dependent carrier generation in the depletion layer of *p-n* junction contributes markedly to the reverse current only in the low-bias region (|*V*|<0.3 V). As the *reverse* bias voltage increases the current demonstrates an extraordinary weak dependence on temperature and superlinearly increasing with voltage. This behavior can be assumed to be caused by strong electric field effects, i.e. carrier *tunneling* and *impact ionization* of lattice atoms in the depletion layer. The photoelectric measurements make it possible to evaluate the role of these effects. Fig. 8 shows the voltage dependences of the current excited by infrared irradiation of the sample at 80 and 140 K. At low reverse bias, the photocurrent exhibits its saturation, i.e. no impact ionization occurs, while at higher biases (>0.3V) the photocurrent increases drastically that is indicative of the impact ionization process. As expected, carrier multiplication is depressed when temperature rises (see Fig. 8(b)).

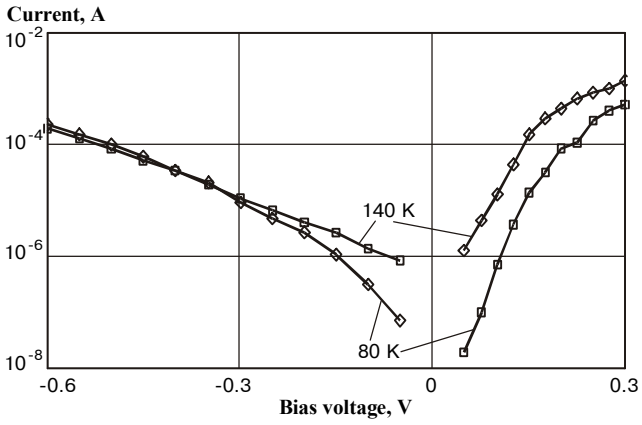

Fig. 7. $Hg_{0,91}Mn_{0,09}$ diode current-voltage characteristics at 80 and 140 K.

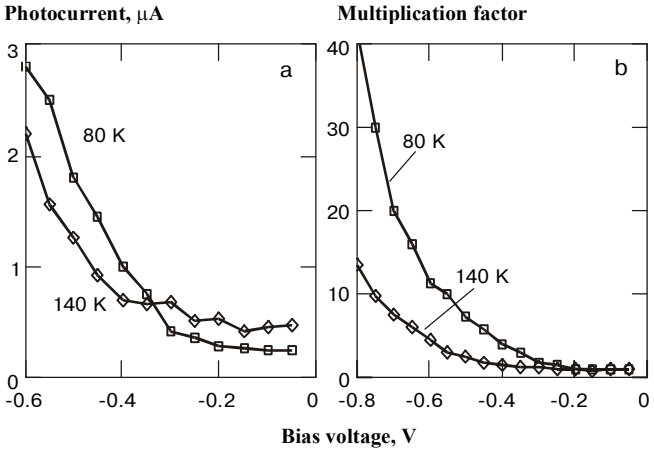

Fig. 8. Photocurrent and multiplication factor voltage dependencies at 80 and 140 K.

Conclusions

The studied *p*-type $Hg_{1-x}Mn_xTe$ (x = 0.1–0.2) alloys are transformed into *n*-type as the temperature increases in the range 80 to 300 K: the greater is the acceptor concentration and the wider is the semiconductor bandgap, the higher is the inversion temperature. This behavior as well as the observed temperature dependence of conductivity are caused by increasing the role of electrons whose mobility is greater by about two order than that of holes.

Intrinsic absorption in $Hg_{1-x}Mn_xTe$ is described adequately in terms of the two-band Kane model with allowance made for the temperature dependence of both the bandgap and effective electron mass. Free-carrier absorption dominates the optical transmission in the below-gap photon energy region. As a result of degeneracy, easily occurring in *n*-type narrow-gap $Hg_{1-x}Mn_xTe$, the Burstein-Moss shift manifests itself for this material.

The $Hg_{1-x}Mn_xTe$ n^+-*p* junction formed by ion etching exhibit good rectifying and stable properties. At low biases, the *I-V* diode characteristic is determined by generation-recombination in the depletion layer of *p-n* junction. At higher reverse biases, carrier tunneling and avalanche processes come into play causing further increase in the current.

Rererences

1. A. Wall, C. Caprile and A. Franciosi, New ternary semiconductors for infrared application: $Hg_{1-x}Mn_xTe$ // *J. Vac. Sci.Technol.* **A4** (3), pp. 818-822 (1986).
2. R. Tribolet, Alternative small gap materials for IR detection // *Semicond. Sci. Technol.* **5**, pp. 1073-1079 (1990).
3. A. Rogalski, $Hg_{1-x}Mn_xTe$ as a new infrared detector material // *Infrared Phys.* **31** (2), pp. 117-166 (1991).
4. J.K. Furdyna, Electrical, optical, and magnetic properties of $Hg_{1-x}Mn_xTe$ // *J. Vac. Sci. Technol.* **21**(1), pp. 220-228 (1982).
5. J. Kaniewski and A. Mycielski, Optical absorption in $Hg_{1-x}Mn_xTe$, x<0.2 mixed crystals // *Solid State Communications*, **41**(12), pp. 959-962 (1982).

6. P. Becla, Infrared photovoltaic detectors utilizing $Hg_{1-x}Mn_xTe$ and $Hg_{1-x-y}Cd_xMn_yTe$ alloys // *J. Vac. Sci. Technol.* **A4(**4), pp. 2014-2020 (1986).
7. O.A. Bodnaruk, I.M. Gorbatyuk, S.E. Ostapov and I.M. Rarenko, Growth and structure perfection of cadmium-mercury and manganese-mercury chalcogenides // *Inorganic Materials*. **31**(10), pp. 1347-1351 (1995).
8. Sun Weiguo, L.A. Kosyachenko and I.M. Rarenko, Anodic fluoride on $Hg_{1-x}Mn_xTe$ // *J. Vac. Sci. Technol.* **A15(**4), pp. 2202-2206 (1997).
9. L.A. Kosyachenko, I.M. Rarenko, O.A. Bodnaruk, Sun Weiguo and Lu Zheng Xiong, Generation-recombination, tunnel and avalanche processes in $Hg_{1-x}Mn_xTe$-based p-n junctions // *Bulletin of Chernovtsy University. Physics*. (40), pp. 59-64 (1998).
10. E.O. Kane, Band structure of indium antimonide // *J. Phys. Chem. Solids*. **1**, pp. 249-261 (1957).
11. B.L. Gelmgolt, V.I. Ivanov-Omslii and I.M. Tsidilkovskii, Electronic energy spectrum of gapless semiconductors // *Uspekhi Fiz. Nank,* **120(**3), pp. 337-362 (1976).
12. M.D. Blue, Optical absorption in HgTe and HgCdTe // *Phys. Rev.* **134** (1A), pp. A226-A234 (1964).
13. E. Janik and G. Karczewski, Carrier transport mechanism in $Hg_{1-x}Mn_xTe$ photovoltaic diodes // *Acta Physica Polonica,* **A73** (3), pp.439-442 (1988).
14. P. Brogowski, H. Mucha and J. Piotrowski, Modification of mercury cadmium telluride, mercury manganese telluride and mercury zinc telluride by ion etching // *Phys. Stat. Sol. (a),* **114**, pp. K37-K40 (1989).